An Interharmonic Phasor and Frequency Estimator for Subsynchronous Oscillation Identification and Monitoring

Lei Chen, Wei Zhao, Fuping Wang, Qing Wang, *Senior Member, IEEE,* and Songling Huang, *Senior Member, IEEE*

Abstract—Recently, subsynchronous oscillations (SSOs) have occurred frequently due to the interaction between wind farm controllers and transmission networks. When an SSO occurs, sub- and supersynchronous interharmonics are present in a voltage/current signal. Because SSOs are serious threats to power system safety and stability, it is important to study sub- and supersynchronous interharmonic phasor and frequency estimators for SSO identification and monitoring (thus for mitigation equipment operation). The systematic errors of the Taylor-Fourier multifrequency model-based parameter estimator are analyzed theoretically. It is found that the key to high estimation accuracy is to select interharmonic and fundamental model frequencies as accurately as possible. To this end, the three-point interpolated discrete Fourier transform and an iteration scheme are used to select initial model frequencies and modify them iteratively. Simulation tests show that the interharmonic total vector error (TVE) and frequency error (FE) of the proposed method are always below 0.6% and 25 mHz, respectively. The fundamental TVE and FE limits in the IEEE standard can also be fully met, and the computation time can meet the requirements of high reporting rate PMUs. Additionally, current samples recorded in an SSO event are used to demonstrate the real benefits of the proposed method.

Index Terms—Digital filter, fundamental phasor, interharmonic phasor, subsynchronous oscillation, Taylor-Fourier multifrequency model.

I. INTRODUCTION

I N recent years, subsynchronous oscillation (SSO) events have occurred frequently in many wind farms [1]. They are caused by the interaction between double-fed induction generators and series compensation-based transmission networks [2], [3]. SSOs can bring severe damages to power system equipment. For example, the electromagnetic effect in SSOs can break make turbine generator shafts [4]. Meanwhile, SSOs can result in abnormal operations of power systems. They are big threats to power system stability and security. As a result, it is of urgency and significance to identify and monitor SSOs for SSO mitigation equipment design and operation.

Typically, when an SSO event occurs, a subsynchronous interharmonic (within [0, 50] Hz) and a supersynchronous interharmonic (within [50, 100] Hz) will be present simultaneously in voltages/currents [5], [6]. Their magnitudes and frequencies can be time-variant, and their frequencies are symmetrical with respect to fundamental frequency [6]. In this case, measurement of interharmonic phasor and frequency becomes a very difficult problem. The interharmonics with close frequencies can have mutual interferences on their parameter measurement, and the dynamic behaviors of these parameters make it more difficult.

Phasor measurement units (PMUs) are widely used in power systems for synchrophasor (called fundamental phasor in the following) estimation [7]. However, these instruments cannot obtain interharmonic parameter estimates. In China, PMU is also expected to play an important role in SSO identification and monitoring, i.e., measuring interharmonics within [10, 40] and [60, 90] Hz [8]. This is because most interharmonics caused by SSOs have frequencies within these two bands [9]. Concerning SSO identification and monitoring, the key is to obtain sub- and supersynchronous interharmonic phasors and frequencies for mitigation equipment operation [10]. The goal of this paper is to propose an interharmonic phasor and frequency estimator with high accuracy, low computational complexity (thus high reporting rate) and short latency.

There are two kinds of sub-/supersynchronous interharmonic parameter estimation methods in literature: 1) fundamental phasor estimates-based methods and 2) signal field data-based methods. As for 1), two typical methods were proposed in [9] and [10] to identify SSOs. Nevertheless, they have an extremely long latency due to the long observation window, which reaches 1 s. [6] proposed a method to estimate SSO frequencies based on the fundamental phasor estimates. However, it cannot estimate sub-/supersynchronous interharmonic phasors.

Concerning 2), a widely used tool is the discrete Fourier transform (DFT). However, it relies on a long observation window to get high frequency resolutions. When a short window is used, the spectrum of an interharmonic will be significantly interfered by the spectral leakage from fundamental and other interharmonics. In this way, large errors are unavoidable. The compressive sensing (CS)-DFT can suppress mutual interferences by using a multisine signal model [11]. However, this static phasor model-based method is not suitable for dynamic interharmonic parameter estimation. The CS of Taylor-Fourier multifrequency (CSTFM)

describes dynamic phasors based on the Taylor expansion model. [12]–[15]. It can obtain interharmonic phasor derivative estimates, and thus interharmonic phasors and frequencies. However, it relies on a large number of iterations to obtain these estimates. As a result, remarkable computations are needed, which is not suitable for high reporting rate PMUs. In order to deal with this problem, a fast version of the CSTFM (i.e., the fast-TFM) was proposed in [16]. The fast-TFM needs to precompute interharmonic and harmonic model frequencies based on the zero-padding DFT. When there are several components within [10, 90] Hz, the sub- or supersynchronous interharmonic model frequencies cannot be selected accurately due to the mutual interferences. This incorrect signal model will lead to large errors. Moreover, the systematic errors relating to model frequency accuracy have not been analyzed yet in [16]. In [1], a bandpass digital filter-based method was proposed for interharmonic parameter estimation. This method uses the 50cycle DFT to precompute interharmonic frequencies and then design filters. Obviously, this extremely long data window will lead to a long latency.

In [17], an interharmonic phasor estimator (called the iterative-TFM in this paper) was proposed. It selected initial model frequencies based on the windowed DFT (WDFT) and modified them based on the phasor derivative estimates. In this paper, a significantly improved version of the iterative-TFM (called the improved iterative-TFM, I²TFM) is proposed to achieve two excellent properties. The first one is the strong harmonic suppression. Low-order harmonics are considered in the signal model to achieve a notch filter effect around these harmonic frequencies. Also, a window function is adopted to weight the samples for high-order harmonic suppression. The second one is the accurate selection of model frequencies. Systematic errors of the I²TFM are analyzed first. It is found that the key to high estimation accuracy is to select model frequencies as accurately as possible. The I²TFM uses the three-point interpolated DFT (IpDFT) [18] to accurately find initial model frequencies, and iteratively modifies them by frequency estimates. As a result, high accuracy is achieved in phasor and frequency estimation. Unlike the fast-TFM, a static harmonic phasor model is used in the I²TFM, which makes the model matrix significantly reduced. Besides, only three iterations are needed to modify model frequencies. Thus, the computation time is short enough to meet high reporting rate PMU requirements. Because the observation window is quite short, the reporting latency is also short.

II. INTRODUCTION OF THE I²TFM

In this section, the I²TFM is introduced. Firstly, the signal model is founded. Then, the least square method for phasor derivative estimation is proposed. Next, systematic errors of the proposed method are analyzed, and the key to high estimation accuracy is pointed out. Afterwards, the approach for accurate model frequency selection is proposed. Finally, the implementation steps of the proposed method are summarized.

A. Signal Model

As stated in section I, when an SSO occurs, a subsynchronous interharmonic and a supersynchronous interharmonic will be present in voltages/currents. Harmonics can also be present, especially in currents. In this way, the signal model can be designed as follows.

$$s(t) = \mathrm{Re}\{a_1(t)e^{j(2\pi ft+\phi_1(t))} + a_{\mathrm{sub}}(t)e^{j(2\pi f_{\mathrm{sub}}t+\phi_{\mathrm{sub}}(t))}$$
$$+ a_{\mathrm{sup}}(t)e^{j(2\pi f_{\mathrm{sup}}t+\phi_{\mathrm{sup}}(t))} + \sum_{h=2}^{H} a_h e^{j(2\pi hft+\phi_h)}\}$$
(1)

where $\mathrm{Re}\{\cdot\}$ denotes the operation of picking the real part of its argument; $a_1(t)$, $a_{\mathrm{sub}}(t)$, $a_{\mathrm{sup}}(t)$ and a_h, with $h = 2,...,H$, are the amplitudes of fundamental, subsynchronous interharmonic, supersynchronous interharmonic and hth harmonic, respectively; $\varphi_1(t)$, $\varphi_{\mathrm{sub}}(t)$, $\varphi_{\mathrm{sup}}(t)$ and φ_h, with $h = 2,...,H$, are the phases of fundamental, subsynchronous interharmonic, supersynchronous interharmonic and hth harmonic components, respectively; and f, f_{sub} and f_{sup} are the frequencies of fundamental, subsynchronous interharmonic and supersynchronous interharmonic, respectively. Please note that the harmonic amplitudes and phases are assumed as static values. Thus, the model matrix (see (6)) can be significantly reduced because of the simplified model on harmonics, which are assumed dynamic in [16]. Only low-order harmonics are considered in the signal model. High-order harmonics are suppressed by adopting a window function (see (7)). The computational complexity will be significantly reduced too. The sub- and supersynchronous interharmonic phasors are defined as

$$p_{\mathrm{sub}}(t) = \frac{a_{\mathrm{sub}}(t)}{\sqrt{2}}e^{j\phi_{\mathrm{sub}}(t)}$$
$$p_{\mathrm{sup}}(t) = \frac{a_{\mathrm{sup}}(t)}{\sqrt{2}}e^{j\phi_{\mathrm{sup}}(t)}$$
(2)

According to the IEEE standard C37.118.1-2011 [19], a fundamental phasor (synchrophasor) is defined as a phasor referred to the nominal fundamental frequency f_0, which is given by

$$x_1(t) = \frac{a_1(t)}{\sqrt{2}}e^{j(2\pi(f-f_0)t+\phi_1(t))}$$
$$= p_1(t)e^{j2\pi(f-f_0)t}$$
(3)

where $p_1(t) = \frac{a_1(t)}{\sqrt{2}}e^{j\phi_1(t)}$ is the so called the raw fundamental phasor. Similarly, $p_h = \frac{a_h}{\sqrt{2}}e^{j\phi_h}$ is defined as the hth harmonic phasor. The Taylor expansion model is used to

describe raw dynamic fundamental phasor [20], which is given by

$$p_1(t) = p_{1,0} + t \cdot p_{1,1} +, ..., + \frac{t^K}{K!} \cdot p_{1,K}$$
$$-\frac{T_w}{2} \le t \le \frac{T_w}{2} \qquad (4)$$

where $p_{1,k}$ is the kth derivative of the phasor $p_1(t)$ at $t = 0$, and T_w is the length of the observation window. Interharmonic phasors $p_{sub}(t)$ and $p_{sup}(t)$ can also be modelled based on the Taylor series, and is truncated to the Lth and Zth order, respectively. Please note that the Taylor model for fundamental and interharmonics can be truncated to different orders of K, L and Z. In this way, (1) can be approximately expressed as

$$s^K(t) = \sqrt{2}\text{Re}\{\sum_{h=2}^{H} p_h e^{j2\pi h f t} + \sum_{l=0}^{L} \frac{t^l}{l!} p_{sub,l} e^{j2\pi f_{sub} t}$$
$$+ \sum_{z=0}^{Z} \frac{t^z}{z!} p_{sup,z} e^{j2\pi f_{sup} t} + \sum_{k=0}^{K} \frac{t^k}{k!} p_{1,k} e^{j2\pi f t}\} \qquad (5)$$
$$-\frac{T_w}{2} \le t \le \frac{T_w}{2}$$

B. Least Square Method

Assume (1) is sampled at sampling rate $f_s = f_0 N_0$, where N_0 is the sample number in one nominal cycle; and N_w samples are obtained in the observation window $[-\frac{T_w}{2}, \frac{T_w}{2}]$. Please note that in order to make $t = 0$ at the center of the observation window, N_w should be an odd number. $c = \lfloor \frac{N_w}{N_0} \rfloor$ is the integer cycle of the observation window, where $\lfloor \cdot \rfloor$ denotes the operation of selecting the closest integer of its argument. After sampling, (5) can be rearranged as

$$s \approx \frac{\sqrt{2}}{2} \begin{bmatrix} \psi & \psi^* \end{bmatrix} \begin{bmatrix} p \\ p^* \end{bmatrix} = \frac{\sqrt{2}}{2} \Psi P \qquad (6)$$

where $p \in C^{(K+L+Z+3)+(H-1)}$ is a column vector consisting of the phasor derivatives $p_{1,k}$, $p_{sub,l}$, $p_{sup,z}$ and harmonic phasor p_h; $p^* \in C^{(K+L+Z+3)+(H-1)}$ is the conjugate column vector of p; $\psi \in \mathcal{C}^{N_w \times [(K+L+Z+3)+(H-1)]}$ is a matrix consisting of N_w samples of bases $\frac{t^k}{k!}e^{j2\pi f t}$, $\frac{t^l}{l!}e^{j2\pi f_{sub} t}$, $\frac{t^z}{z!}e^{j2\pi f_{sup} t}$ and $e^{j2\pi h f t}$; $\psi^* \in C_{N_w \times [(K+L+Z+3)+(H-1)]}$ is the conjugate matrix of ψ; and $s \in R^{N_w}$ is a column vector with N_w samples of $s(t)$.

The least square method can be used to estimate the matrix P (thus interharmonic and fundamental derivatives), and a window function is adopted to suppress higher order harmonic interferences, which is given by

$$W s \approx \frac{\sqrt{2}}{2} W \Psi P \qquad (7)$$

$$\hat{P} \approx \sqrt{2}(\Psi^H W^H W \Psi)^{-1} \Psi^H W^H W s \qquad (8)$$

where W is a diagonal matrix generated by the window function, and H denotes the operation of Hermitian. In this paper, the fourth-order Kaiser window is adopted because of its good passband and stopband performances [21].

Accordingly, the zeroth-order phasor derivatives are the interharmonic phasors and raw fundamental phasor estimates, and the fundamental phasor can be obtained according to (3). According to [22], the subsynchronous interharmonic frequency can be estimated based on the phasor derivative estimates, which is given by

$$\hat{f}_{sub} = f_{sub} + \frac{1}{2\pi} \frac{\text{Im}\{p^*_{sub,0} p_{sub,1}\}}{|p_{sub,0}|^2} \qquad (9)$$

where $\text{Im}\{\cdot\}$ denotes the operation of picking the imaginary part of its argument; and $*$ denotes the conjugate operator. Similarly, supersynchronous interharmonic and fundamental
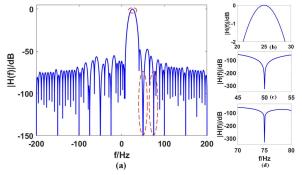

Fig. 1. Frequency response of the equivalent filter for $p_{sub,0}$ estimation. Model frequencies are set at $f = 50$ Hz, $f_{sub} = 25$ Hz and $f_{sup} = 75$ Hz. $c = 8$ is selected for illustration. (b) for frequency response around $f = 25$ Hz; (c) for frequency response around $f = 50$ Hz; and (d) for frequency response around $f = 75$ Hz.

frequencies can be estimated like (9). Fundamental rate of change of frequency (ROCOF) can be estimated by [22]

$$R\hat{O}COF = \frac{1}{2\pi} \frac{\text{Im}\{p^*_{1,0} p_{1,2}\}}{|p_{1,0}|^2} - \frac{1}{\pi} \frac{\text{Re}\{p^*_{1,0} p_{1,1}\}\text{Im}\{p^*_{1,0} p_{1,1}\}}{|p_{1,0}|^4} \qquad (10)$$

C. Key to High Estimation Accuracy

This section analyzes the systematic error of the I^{2}TFM theoretically. Then the key to high accuracy is pointed out. Generally, the I^{2}TFM can be seen as a bank of finite-impulseresponse filters for phasor derivative estimation. For example, the equivalent filter $h_{sub}(n)$ (with $n = 0,..,N_w-1$) for $p_{sub,0}$ estimation is the time-inverse version of the corresponding row of matrix $(\Psi^H W^H W \Psi)^{-1} \Psi^H W^H W$ [21]. Assume the frequency response of filter $h_{sub}(n)$ is $H_{sub}(f)$.

Under steady-state conditions, the total vector error (TVE) upper bound of the equivalent filter is (see Appendix A)

$$
\begin{aligned}
TVE_{\text{sub}}^{\max} = {} & |H_{\text{sub}}(f_{\text{sub}}) - 1)| + |H_{\text{sub}}(-f_{\text{sub}})| \\
& + r_1(|H_{\text{sub}}(f)| + |H_{\text{sub}}(-f)|) \\
& + r_{\text{sup}}(|H_{\text{sub}}(f_{\text{sup}})| + |H_{\text{sub}}(-f_{\text{sup}})|) \\
& + \sum_{h=2}^{H} r_h(|H_{\text{sub}}(hf)| + |H_{\text{sub}}(-hf)|)
\end{aligned}
\tag{11}
$$

where $r_1 = \frac{|p_1|}{|p_{\text{sub}}|}$, $r_{\text{sup}} = \frac{|p_{\text{sup}}|}{|p_{\text{sub}}|}$ and $r_h = \frac{|p_h|}{|p_{\text{sub}}|}$ are the ratios of fundamental, supersynchronous interharmonic and hth harmonic magnitudes to subsynchronous interharmonic magnitude, respectively. Please note that under steady-state conditions, the sub-/supersynchronous interharmonic and raw fundamental phasors are static values.

From Appendix A and (11), we can see that the subsynchronous interharmonic TVE (or systematic error) of the proposed estimator is affected by two factors: 1) passband performances, which are mainly determined by the passband gain $H_{\text{sub}}(f_{\text{sub}})$; and 2) stopband performances, which mainly depend on the stopband gain, i.e., $H_{\text{sub}}(-f_{\text{sub}})$, $H_{\text{sub}}(f)$, $H_{\text{sub}}(-f)$, etc.

In practice, the actual sub-/supersynchronous interharmonic and fundamental frequencies are unknown. Thus, the model
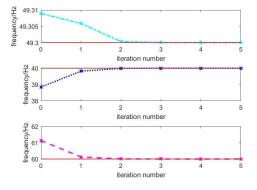

Fig. 2. Frequency estimates at each iteration. 10% sub- and supersynchronous interharmonics are added to a pure sine signal. f_{sub} = 40 Hz, f = 49.3 Hz, f_{sup} = 60 Hz, $K = 2$, $L = Z = 1$ and $c = 8$ are selected for illustration. The initial model frequencies are placed at the zeroth iteration. The red continuous lines denote the actual frequencies.

frequencies used to generate matrix $\mathbf{\Psi}$ may be not equal to the actual ones. According to Fig. 1(b) and (A5), when the actual subsynchronous interharmonic frequency is close to the model frequency, $H_{\text{sub}}(f_{\text{sub}}) \to 1$. When the actual supersynchronous interharmonic and fundamental frequencies are close to the corresponding model frequencies, $H_{\text{sub}}(f_{\text{sup}}) \to 0$, $H_{\text{sub}}(f) \to 0$ (see Fig. 1(c), (d) and (A5)). In addition, the frequency responses around negative model frequencies and harmonic frequencies have the same performances, e.g., $H_{\text{sub}}(-f_{\text{sub}}) \to 0$. In this case, $TVE_{\text{sub}}^{\max}$ (or systematic error) $\to 0$. Thus, the key to high estimation accuracy is to select model frequencies as

accurately as possible. The closer the model frequencies are to the actual ones, the more ideal the filter's performances are.

D. Initial Model Frequency Selection and Modification

At first, the Hanning window-based three-point IpDFT (see Appendix B) is used to estimate fundamental phasor and frequency [18]. Obviously, the three-point IpDFT is more accurate than the WDFT used in [17], and is more robust to interharmonic interferences than the two-point IpDFT. In addition, the three-point IpDFT is much lighter than the zeropadding DFT used in [16].

Then, these estimates are used to generate the fundamental and remove it from the original signal. Next, sub- and supersynchronous interharmonic frequencies are estimated by the Hanning window-based three-point IpDFT. Similarly, the three-point IpDFT is more robust to residual fundamental interferences than the two-point IpDFT.

Please note that these initial model frequencies have errors because of the unavoidable interferences from other components. They are iteratively modified by the frequency estimates. At first, the initial model frequencies are used to generate matrix $\mathbf{\Psi}$ and get phasor derivative estimates. Then, these phasor derivative estimates are used to estimate frequencies according to (9). Finally, model frequencies are set equal to these frequency estimates and generate matrix $\mathbf{\Psi}$. Iterations of the last two steps are needed to get accurate model frequency estimates. The number of iterations should be selected as a tradeoff between the accuracy and computations. Through a large number of simulations, we can conclude that only three iterations are needed to get a high accuracy (see Fig. 2). Moreover, the computation time will be short because of this small number of iterations.

E. Implementation Steps

The implementation steps of the I²TFM are summarized in TABLE I. The proposed method is organized into three parts: 1) initialization; 2) initial model frequency selection and modification; and 3) interharmonic and fundamental parameter estimation. Please note that steps 5 and 6 correspond to the first iteration, and step 7 denotes the second and third iteration for model frequency modification.

TABLE I
IMPLEMENTATION STEPS OF THE I²TFM.

1). Initialization
1. Input data $s(n)$
2. Initialize parameters H, K, L, Z and threshold q
2). Initial model frequency selection and modification

---

1. Obtain $\hat{f}$ and $\hat{p}_1$ based on the three-point IpDFT

2. Generate estimated fundamental signal $\hat{s}_1 = \sqrt{}\ 2\mathrm{Re}\{\hat{p}_1 e^{j2\pi f1\ \hat{}\ t}\}$

3. Remove $\hat{s}_1$ from the original one $s_r(n) = s(n) - \hat{s}_1(n)$

4. Use the three-point IpDFT to obtain $\hat{f}_{sub}$ and $\hat{f}_{sup}$ (see Appendix B)

5. Use $\hat{f}, \hat{f}_{sub}$ and $\hat{f}_{sup}$ to generate matrix Ψ for the I²TFM

6. Obtain $\hat{f}, \hat{f}_{sub}$ and $\hat{f}_{sup}$ according to (9)

7. Do step 5 and 6 two times for another 2 iterations.

3). Interharmonic and fundamental phasor estimations

1. Again, use $\hat{f}, \hat{f}_{sub}$ and $\hat{f}_{sup}$ to generate matrix Ψ for the I²TFM

2. Obtain $\hat{p}_1, \hat{f}, \widehat{ROCOF}, \hat{x}_1, \hat{p}_{sub}, \hat{f}_{sub}, \hat{p}_{sup}$ and $\hat{f}_{sup}$ according to (8), (9) and (3)

III. Computational Burden, Reporting Rate and Latency

The PMU reporting rate is mainly determined by the computation time of its phasor estimation algorithm. In China, the PMU reporting rate (RR) is generally 50 frames per second (fps). Thus, PMU computation time needs to be smaller than 1/50 s. In TABLE II, computations of the I²TFM in different steps are listed. As shown, the main computations of the I²TFM are in step 6, part 2) and step 2, part 3), i.e., in matrix pseudo-inversion and phasor estimation. Assuming f_s = 2000 Hz, K = 2, $L = Z = 1$ and $H = 5$, then the total floatingpoint operations are 5245107 and 5875931 for c = 8 and 9 cycles, respectively.

Texas Instruments Inc. provides a floating-point digital signal processor (DSP) TMS320C6713B with a 200-MHz clock rate [23]. It has an acceptable price and can perform up to 1200 million floating-point operations per second (MFLOPS). If it is used in PMUs, the computation time will be 4.37 and 4.90 ms for an eight- and nine-cycle observation window, respectively. Obviously, they are much shorter than the upper bound (20 ms) for RR=50 fps. Moreover, the I²TFM can even be used for PMUs with the highest reporting rate of 100 fps [19], where the computation time needs to be shorter than 10 ms.

TABLE II

COMPUTATIONS OF THE I²TFM. $\gamma = 2(K + L + Z + 3) + 2(H - 1)$ IS USED FOR EXPRESSION SIMPLIFICATION. THE LU DECOMPOSITION -BASED METHOD IS USED FOR MATRIX INVERSION.

Part	Step	Computation Type	
		cos, sin, ×, ÷	+, −
2)	1	$4N_w$	$4(N_w - 1)$
	2	$4N_w$	0
	3	0	N_w
	4	$8cN_w$	$4c(N_w - 1)$
	5	$[12 + 2(K + L + Z) + 3H]N_w$	0
	6	$(16 + 8\gamma^2)N_w + \frac{20}{3}\gamma^3 + 2\gamma^2 - 2\gamma - \frac{4}{3}\gamma$	$(4\gamma^2 - 2\gamma + 12)N_w + \gamma^3 + \gamma^2 - 8\gamma - 8$
3)	1	$[12 + 2(K + L + Z) + 3H]N_w$	0
	2	$(22 + 8\gamma^2)N_w + \frac{20}{3}\gamma^3 + 2\gamma^2 - 2\gamma - \frac{4}{3}\gamma$	$(4\gamma^2 - 2\gamma + 18)N_w + \gamma^3 + \gamma^2 - 8\gamma - 14$

According to the IEEE standard [19], PMU latency is mainly determined by its observation window and computation time T_c. Because the I²TFM obtains phasor derivative estimates at its center window, its time delay is equal to half of the observation window, i.e., $\frac{1}{2}T_w$. Then the total latency is $\frac{1}{2}T_w + T_c$. When an SSO occurs, it is expected to be identified as soon as possible. If the same parameters in section III are used, then the latency will be 84.37 and 94.90 ms for eightand nine-cycle observation windows, respectively. Obviously, they are much shorter than the latency of the method given in [1], which is longer than 500 ms. In the new IEEE standard [24], the reference estimator for M class PMUs is about nine cycles long (for RR=50 fps). Thus, the eight-cycle I²TFM's latency is also shorter than the reference estimator.

IV. On the Interharmonic Detection Threshold q and Detection Probability

In this paper, the interharmonic detection threshold q is set to 3% of the fundamental. When such a threshold is used, the detection probability for interharmonics with different magnitudes are different. A simulation test is done to count the detection probability. We assume the signal include the fundamental, subsynchronous interharmonic and supersynchronous interharmonic components. The fundamental frequency are set to the nominal value. The subsynchronous interharmonic frequency is set from 10 to 40 Hz in step of 1 Hz. Accordingly, the supersynchronous interharmonic frequency is set from 90 to 60 Hz in step of -1 Hz. The sub- and supersynchronous interharmonic magnitudes can be different, but we set them to the same value (from 4% to 150% of the fundamental in step of 1%) for better clarity. For a certain interharmonic frequency and magnitude, the initial phases of the three components are all randomly selected within [0, 2π] rad in 200 repeated runs.

In Fig. 3, the detection probability of the I²TFM for interharmonics with different magnitudes are shown. For c = 8, only when the interharmonic magnitudes are 4% of the fundamental, the detection probability is a bit smaller than 100%, i.e., 99.56%. In other conditions, the detection probabilities are all 100%. For a longer observation window (c = 9), the interharmonics can always be detected successfully. Such results show the I²TFM has good performances on interharmonic detection.

Fig. 3. Detection probability of the I²TFM for interharmonics with different magnitudes. The sub- and supersynchronous interharmonic magnitudes are both expressed as % of the fundamental ([4%, 150%]).

V. PERFORMANCE TESTS

In this section, several simulation tests and a practical example are carried out for the I²TFM performance evaluation. Basic performances and robustness to various uncertainty contributions, such as fundamental frequency deviation, interharmonic magnitude modulation, interharmonic frequency ramp and harmonic distortion, are tested in this paper. Other interharmonic parameter estimators can have large errors, especially when the two interharmonics have frequencies of 40 and 60 Hz. Thus, no other estimators are used to compare performances with the I²TFM. In order to demonstrate the real benefit of the I²TFM, a practical example is taken. The I²TFM parameters are set the same as those in section III. The phase of each component is set at 0 rad. The IEEE standard requirements on an out-of-band interference test are referred for fundamental phasor measurement [19], [24]. However, as far as we know, there are no references on interharmonic parameter measurement requirements. Each test are simulated over at least 1000 runs.

A. Basic Performance Test

This test is to evaluate the I²TFM's performance under normal conditions. The sub- and supersynchronous interharmonic magnitudes are the same values, which are set from 5% to 150% of the fundamental in steps of 5%. The subsynchronous interharmonic frequency is varied from 10 to 40 Hz in step of 1 Hz. Thus, the supersynchronous interharmonic frequency is set accordingly from 90 to 60 Hz in steps of 1 Hz. Please note that the sub-/supersynchronous interharmonic magnitude can be very great, sometimes even greater than the fundamental magnitude [5]. In this paper, interharmonic magnitudes are set at up to 150% of the fundamental.

The maximum TVE, frequency error (FE) (all in absolute values in the following) and ROCOF error (RFE) (all in absolute

values in the following) are shown in TABLE III. We can see that all errors are null. This is because the interharmonic

TABLE III
MAXIMUM TVEs, FEs AND RFEs IN ALL CASES (NO NOISE)

Comp.	Parameter	basic test	
		$c = 8$	$c = 9$
sub.	max. TVE [%]	0.00	0.00
	max. FE [Hz]	0.00	0.00
sup.	max. TVE [%]	0.00	0.00
	max. FE [Hz]	0.00	0.00
fund.	max. TVE [%]	0.00	0.00
	max. FE [Hz]	0.00	0.00
	max. RFE [Hz/s]	0.00	0.00

and fundamental model frequencies are modified by three iterations, and thus are almost equal to the actual ones. In this case, ideal performances can be obtained. The conclusion drawn in section II-D is well verified.

In another test, additive wideband noise with a signal-tonoise ratio SNR=70 dB is also added to the signal. Obviously, the maximum errors are obtained when $f_{sub} = 40$ Hz and $f_{sup} = 60$. The maximum TVEs, FEs and RFEs under different interharmonic magnitude conditions are shown in Fig. 4. When $c = 8$, the maximum TVEs and FEs of the sub-/supersynchronous interharmonic are well below 0.3% and 15 mHz, respectively. Thus, the I²TFM can accurately estimate interharmonic phasors and frequencies in wide magnitude and frequency bands, i.e., interharmonic magnitudes within [5%, 150%] of the fundamental, and subsynchronous interharmonic frequency within [10, 40] Hz. Because the interferences from wideband noise are larger in small magnitude interharmonics, they will have larger errors in phasor and frequency estimation. As for fundamental parameter estimation, the I²TFM can meet the IEEE standard requirements on TVE (1.3%) and FE (10 mHz) by using an eight-cycle window (RFE limit is suspended in the new IEEE standard [24]).

More importantly, the nine-cycle I²TFM is generally more accurate than the eight-cycle window-based method, i.e., the estimation errors of all parameters can be reduced over a longer observation window.

It is interesting that, with the increase of sub- and supersynchronous interharmonic magnitudes, the interharmonic TVEs and FEs become smaller, whereas the fundamental TVE, FE and RFE become larger. This is because when the interharmonic magnitudes increase, the initial interharmonic frequencies can be determined more accurately, whereas the interharmonic interferences on fundamental parameter estimation become larger.

B. Robustness to Various Uncertainty Contributions

In an SSO, there can be other uncertainty contributions to interharmonic and fundamental parameter estimation, such as fundamental frequency deviation, interharmonic amplitude modulations, interharmonic frequency ramp and harmonic

distortion. In this part, several test cases given below are considered to evaluate the I²TFM's performances. The parameters without specification are selected the same as the second test of section V-A, i.e., 70-dB wideband noise is also considered.

c) Interharmonic frequencies can have linear ramps in anSSO. In this paper, the ramp rate is set at 0.02 Hz/s. In order to simulate the worst condition, the subsynchronous interharmonic frequency is set from 39 to 40 Hz in ramp rate of 0.02 Hz/s, and the supersynchronous interharmonic frequency is accordingly from 61 to 60 Hz in ramp rate of -0.02 Hz/s.

d) Harmonics can also be present in a voltage/current

TABLE IV RESULTS UNDER DIFFERENT TEST CONDITIONS. SNR=70 dB

Comp.	Parameter	a) fund. freq. dev.		b) int. AM		int. freq. ramp		harm. dist.	
		=8	=9	=8	=9	=8	=9	=8	=9
sub.	max. TVE [%]	0.45	0.21	0.33	0.11	0.46	0.21	0.33	0.19
	max. FE [mHz]	19	12	13	9.1	20	11	14	10
sup.	max. TVE [%]	0.29	0.15	0.28	0.14	0.52	0.20	0.34	0.14
	max. FE [mHz]	16	7.7	13	11	20	15	21	10
fund.	max. TVE [%]	0.16	0.06	0.18	0.13	0.23	0.11	0.13	0.06
	max. FE [mHz]	2.8	1.1	1.6	0.7	1.5	0.8	1.3	0.8
	max. RFE [Hz/s]	0.13	0.04	0.12	0.04	0.12	0.05	0.11	0.06

signal.In this part, a signal with 5% third harmonic and 3% fifth harmonic is used for test.

The maximum TVEs, FEs and RFEs under the above test cases are shown in TABLE IV. By comparing with Fig. 4, a series of conclusions can be drawn. Fundamental frequency deviation and interharmonic frequency ramp can increase interharmonic TVEs and FEs. By contrast, interharmonic amplitude modulation and harmonic distortion have little impact on the interharmonic parameter estimation. In all cases, the maximum TVEs and FEs of both interharmonics are always below 0.6% and 25 mHz, respectively. Regarding fundamental parameter estimation, all these four disturbances have little contribution to its uncertainty. The TVEs and FEs can always fully meet the corresponding requirements of the IEEE standard. For all uncertainty contributions, the estimation errors of all parameters can also be reduced over a longer data window.
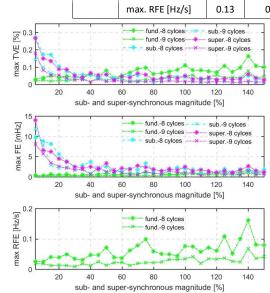

Fig. 4. Maximum TVEs, FEs and RFEs under different interharmonic magnitude conditions (SNR=70 dB). The sub- and supersynchronous interharmonic magnitudes are expressed as percentages of the fundamental.

a) When an SSO occurs, the fundamental frequency maydeviate from the nominal value. For example, in a severe SSO event, the frequency of the western China grid dropped to 49.91 Hz [9]. In [1], a 0.12-Hz deviation is considered for simulation. In this paper, we consider a maximum deviation of 0.7 Hz ($f = 49.3$ Hz) for the severest conditions in China.

b) In an SSO, interharmonic amplitudes can have modulations. In this part, the modulation levels and frequencies of the two interharmonic components are both set at 15% of the interharmonic and 0.15 Hz as an example.

C. A Practical Example

In this section, we use a practical example to demonstrate the benefits of the proposed method. A series of current sampling data recorded by a fault recorder in an SSO event are used for the test, which are shown in Fig. 5(a). Its sampling frequency is 1200 Hz. From its spectrum (see Fig. 5(b)), we can see that a subsynchronous interharmonic ($f_{sub} \approx 23$ Hz) and a supersynchronous interharmonic ($f_{sup} \approx 77$ Hz) are present in the current signal. Their amplitudes are both about 5% of the fundamental.

Because the actual values of all parameters are unknown, the Hanning-based three-point IpDFT is used to compare the performance with the I²TFM. The observation windows of the two methods are both eight cycles long. From Fig. 6 and 7, we can see that the sub- and supersynchronous interharmonics

can be successively detected and monitored by the I²TFM. Moreover, the I²TFM's interharmnonic amplitude and frequency estimates are smoother, whereas the IpDFT's estimates are rough and oscillating due to the interferences from fundamental and other components. The mean signalto-noise (i.e., original signal to the residual) ratios of the I²TFM and IpDFT is 90.85 dB and 24.34 dB, repectively. Such evidence indicates that the I²TFM is much more accurate than the IpDFT.
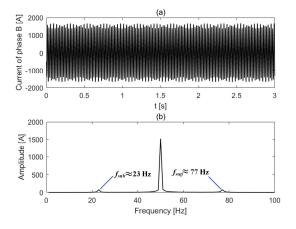

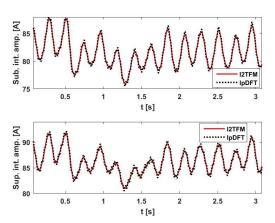Fig. 5.   Current sampling data ((a)) recorded in an SSO event and its spectrum (b).

Fig. 6. Sub- and supersynchronous interharmonic amplitude estimates of the I²TFM and IpDFT.
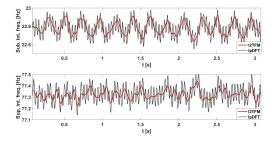

Fig. 7. Sub- and supersynchronous interharmonic frequency estimates of the I²TFM and IpDFT.

VI. CONCLUSION

In this paper, an interharmonic phasor and frequency estimator is proposed for SSO identification and monitoring. Through systematic error analysis, we find that the key to high accuracy is to select model frequencies as accurately as possible. Based on the three-point IpDFT and an iteration scheme, the model frequencies are selected and iteratively modified for high accuracy. Simulation tests show that, by using an eight-cycle observation window, the maximum interharmnonic TVE and FE are always smaller than 0.6% and 25 mHz, respectively. Meanwhile, the computation time is only 4.37 ms, which can even meet the requirements of the highest reporting rate PMUs, i.e., RR=100 fps. The latency is 83.47 ms, which is shorter than the IEEE standard reference method for M class PMUs. Wideband noise, fundamental frequency deviation and interharmonic frequency ramp have the most significant impacts on interharmonic parameter estimation, whereas these effects can be reduced over a longer window. Regarding fundamental parameter estimation, the corresponding IEEE standard requirements can always be fully met.

APPENDIX A

PROOF OF (11)

Under steady-state conditions, the sub-/supersynchronous interharmonic and raw fundamental phasors are all static values. In this way, the output of the filter $h_{\mathrm{sub}}(n)$ on $s(n)$ can be expressed as

$$
\begin{aligned}
\hat{p}_{\mathrm{sub}} &= s(n) * h_{\mathrm{sub}}(n) \\
&= p_{\mathrm{sub}} H_{\mathrm{sub}}(f_{\mathrm{sub}}) + p_{\mathrm{sub}}^* H_{\mathrm{sub}}(-f_{\mathrm{sub}}) \\
&\quad + p_1 H_{\mathrm{sub}}(f) + p_1^* H_{\mathrm{sub}}(-f) \\
&\quad + p_{\mathrm{sup}} H_{\mathrm{sub}}(f_{\mathrm{sup}}) + p_{\mathrm{sup}}^* H_{\mathrm{sub}}(-f_{\mathrm{sup}}) \\
&\quad + \sum_{h=2}^{H} \left(p_h H_{\mathrm{sub}}(hf) + p_h^* H_{\mathrm{sub}}(-hf) \right)
\end{aligned} \tag{A1}
$$

where $*$ denotes the linear convolution. Thus, the TVE of the equivalent filter is [25]

$$
\begin{aligned}
TVE_{\mathrm{sub}} &= \frac{|\hat{p}_{\mathrm{sub}} - p_{\mathrm{sub}}|}{|p_{\mathrm{sub}}|} \\
&= \frac{|p_{\mathrm{sub}}(H_{\mathrm{sub}}(f_{\mathrm{sub}}) - 1) + \eta|}{|p_{\mathrm{sub}}|} \\
&\leq |H_{\mathrm{sub}}(f_{\mathrm{sub}}) - 1| + |H_{\mathrm{sub}}(-f_{\mathrm{sub}})| \\
&\quad + r_1 (|H_{\mathrm{sub}}(f)| + |H_{\mathrm{sub}}(-f)|) \\
&\quad + r_{\mathrm{sup}} (|H_{\mathrm{sub}}(f_{\mathrm{sup}})| + |H_{\mathrm{sub}}(-f_{\mathrm{sup}})|) \\
&\quad + \sum_{h=2}^{H} r_h (|H_{\mathrm{sub}}(hf)| + |H_{\mathrm{sub}}(-hf)|)
\end{aligned} \tag{A2}
$$

where

$$\begin{aligned}\eta = {}& p_{\text{sub}}^* H_{\text{sub}}(-f_{\text{sub}}) + p_1 H_{\text{sub}}(f) + p_1^* H_{\text{sub}}(-f) \\ & + p_{\text{sup}} H_{\text{sub}}(f_{\text{sup}}) + p_{\text{sup}}^* H_{\text{sub}}(-f_{\text{sup}}) \\ & + \sum_{h=2}^{H} (p_h H_{\text{sub}}(hf) + p_h^* H_{\text{sub}}(-hf)) \end{aligned} \qquad (A3)$$

shows the stopband responses of the filter; and $r_1 = \frac{|p_1|}{|p_{\text{sub}}|}$, $r_{\text{sup}} = \frac{|p_{\text{sup}}|}{|p_{\text{sub}}|}$ and $r_h = \frac{|p_h|}{|p_{\text{sub}}|}$ are the ratios of the subsynchronous interharmonic magnitude to the fundamental, supersynchronous interharmonic and hth harmonic magnitudes, respectively. Thus, the TVE upper bound is

$$\begin{aligned}TVE_{\text{sub}}^{\max} = {}& |H_{\text{sub}}(f_{\text{sub}}) - 1| + |H_{\text{sub}}(-f_{\text{sub}})| \\ & + r_1(|H_{\text{sub}}(f)| + |H_{\text{sub}}(-f)|) \\ & + r_{\text{sup}}(|H_{\text{sub}}(f_{\text{sup}})| + |H_{\text{sub}}(-f_{\text{sup}})|) \\ & + \sum_{h=2}^{H} r_h(|H_{\text{sub}}(hf)| + |H_{\text{sub}}(-hf)|) \end{aligned} \qquad (A4)$$

According to [26], when the model frequencies are equal to the actual ones, we can obtain

$$\begin{aligned}& H_{\text{sub}}(f_{\text{sub}}) = 1; \\ & H_{\text{sub}}(-f_{\text{sub}}) = H_{\text{sub}}(f) = H_{\text{sub}}(-f) = H_{\text{sub}}(f_{\text{sup}}) \quad (A5) \\ & = H_{\text{sub}}(-f_{\text{sup}}) = H_{\text{sub}}(hf) = H_{\text{sub}}(-hf) = 0 \end{aligned}$$

APPENDIX B BRIEF INTRODUCTION OF THE THREE-POINT IPDFT

The DFT of $s(n)$ is

$$S(m) = \frac{1}{N_{\text{w}}} \sum_{n=-\frac{N_{\text{w}}-1}{2}}^{\frac{N_{\text{w}}-1}{2}} w(n) s(n) e^{-j2\pi \frac{n}{N_{\text{w}}} m} \qquad (B1)$$

where $w(\cdot)$ is the Hanning window; and $m = 0,\dots,N_{\text{w}} - 1$ is the bin number. The peak bin is found in bins from 0 to $c - 1$. If the peak magnitude is larger than a threshold q, a subsynchronous interharmonic will be considered in the signal model. The corresponding bin number is assumed to be M. Then a fractional compensation term δ can be computed by interpolating three bins $M - 1$, M and $M + 1$, which is given by

$$\delta = \frac{|S(M+1)| - |S(M-1)|}{|S(M+1)| + 2|S(M)| + |S(M-1)|} \qquad (B2)$$

The subsynchronous interharmonic frequency, amplitude and phase can be estimated by

$$\hat{f}_{\text{sub}} = (M + \delta) \frac{f_s}{N_{\text{w}}} \qquad (B3)$$

$$\hat{A}_{\text{sub}} = |S(M)| \frac{\pi\delta}{\sin(\pi\delta)} (\delta^2 - 1) \qquad (B4)$$

$$\hat{\phi}_{\text{sub}} = \angle S(M) - \pi\delta \qquad (B5)$$

Similarly, the supersynchronous interharmonic frequency can be obtained by finding the peak bin in bins from $c + 1$ to $2c$ and estimating frequency according to (B2) and (B3). Fundamental frequency, amplitude and phase can be obtained by finding the peak bin in bins from $c-1$ to $c+1$ and estimating the parameters based on the above equations.

REFERENCES

[1] X. Xie, H. Liu, Y. Wang, Z. Xu, and J. He, "Measurement of suband supersynchronous phasors in power systems with high penetration of renewables," in *Proc. IEEE PES Innov. Smart Grid Technol. Conf. (ISGT)*, Minneapolis, MN, USA, Sept. 2016, pp. 1–5.

[2] X. Xie, X. Zhang, H. Liu, H. Liu, Y. Li, and C. Zhang, "Characteristic analysis of subsynchronous resonance in practical wind farms connected to series-compensated transmissions," *IEEE Trans. Energy Convers.*, vol. 32, no. 3, pp. 1117–1126, 2017.

[3] R. K. Varma, S. Auddy, and Y. Semsedini, "Mitigation of subsynchronous resonance in a series-compensated wind farm using facts controllers," *IEEE Trans. Power Del.*, vol. 23, no. 3, pp. 1645–1654, 2008.

[4] P. Zhang, T. Bi, S. Xiao, and A. Xue, "An online measurement approach of generators torsional mechanical damping coefficients for subsynchronous oscillation analysis," *IEEE Trans. Power Syst.*, vol. 30, no. 2, pp. 585–592, 2015.

[5] H. Liu, J. Li, T. Bi, S. Xu, and Q. Yang, "Subsynchronous and supersynchronous inter-harmonic identification method based on phasor measurements," *Power System Technology*, vol. 41, no. 10, pp. 3237– 3243, 2017.

[6] T. Rauhala, A. M. Gole, and P. Jrventausta, "Detection of subsynchronous torsional oscillation frequencies using phasor measurement," *IEEE Trans. Power Del.*, vol. 31, no. 1, pp. 11–19, 2016.

[7] A. G. Phadke and J. S. Thorp, *Synchronized Phasor Measurements and Their Applications*. Springer US, 2008.

[8] State Grid Corporation of China, "Standardization technical specification for synchronized phasor measurement device in substation," unpublished.

[9] H. Liu, T. Bi, J. Li, S. Xu, and Q. Yang, "An inter-harmonics monitoring method based on PMUs," *IET Gen. Transm. Distrib.*, vol. 11, no. 18, 2017.

[10] F. Zhang, L. Cheng, W. Gao, and R. Huang, "Synchrophasors-based identification for subsynchronous oscillations in power systems," *IEEE Trans. Smart Grid*, vol. PP, no. 99, pp. 1–1, Jan. 2018.

[11] M. Bertocco, G. Frigo, C. Narduzzi, and F. Tramarin, "Resolution enhancement by compressive sensing in power quality and phasor measurement," *IEEE Trans. Instrum. Meas.*, vol. 63, no. 10, pp. 2358–2367, Oct. 2014.

[12] M. Bertocco, G. Frigo, C. Narduzzi, C. Muscas, and P. A. Pegoraro, "Compressive sensing of a Taylor-Fourier multifrequency model for synchrophasor estimation," *IEEE Trans. Instrum. Meas.*, vol. 64, no. 12, pp. 3274–3283, Dec. 2015.

[13] G. Frigo, G. Giorgi, M. Bertocco, and C. Narduzzi, "Multifunction phasor analysis for distribution networks," in *Proc. IEEE Int. Workshop on Appl. Meas. Power Syst. (AMPS)*, Aachen, Germany, Sept 2016, pp. 1–6.

[14] G. Frigo, G. Giorgi, and C. Narduzzi, "Efficient detection for multifrequency dynamic phasor analysis," in *Proc. IEEE Int. Workshop on Appl. Meas. Power Syst. (AMPS)*, Aachen, Germany, Sept 2016, pp. 1–6.

[15] M. Bertocco, G. Frigo, G. Giorgi, and C. Narduzzi, "Frequency tracking for efficient phasor measurement based on a CSTFM model," in *Proc. IEEE Int. Workshop on Appl. Meas. Power Syst. (AMPS)*, Aachen, Germany, Sept 2015, pp. 84–89.

[16] C. Narduzzi, M. Bertocco, G. Frigo, and G. Giorgi, "Fast-TFM–multifrequency phasor measurement for distribution networks," *IEEE Trans. Instrum. Meas.*, vol. 67, no. 8, pp. 1825–1835, Aug. 2018.

[17] L. Chen, W. Zhao, Y. Yu, and S. Huang, "Interharmonic and fundamental phasor estimator for smart grid applications," in *Proc. Conf. Prec. Electrom. Meas. (CPEM)*, Paris, France, Jul. 2018, pp. 1–2.

[18] D. Agrez, "Weighted multipoint interpolated dft to improve ampliture estimation of multifrequency signal," *IEEE Trans. Instrum. Meas.*, vol. 2, no. 2, pp. 998–1003, Feb. 2002.

[19] "IEEE standard for synchrophasor measurements for power systems," *IEEE Std C37.118.1-2011 (Revision of IEEE Std C37.118-2005)*, pp. 1–61, Dec. 2011.

[20] J. A. D. L. O. Serna, "Dynamic phasor estimates for power system oscillations," *IEEE Trans. Instrum. Meas.*, vol. 56, no. 5, pp. 1648–1657, May 2007.

[21] M. A. Platas-Garza, J. Platas-Garza, and J. A. D. L. O. Serna, "Dynamic phasor and frequency estimates through maximally flat differentiators," *IEEE Trans. Instrum. Meas.*, vol. 59, no. 7, pp. 1803–1811, Jul. 2010.

[22] L. Chen, W. Zhao, Y. Yu, Q. Wang, and S. Huang, "Improved interpolated dynamic dft synchrophasor estimator considering second harmonic interferences," in *Proc. IEEE Int. Instrum. Meas. Technol. Conf. (I2MTC)*, Houston, TX, USA, May 2018, pp. 1–6.

[23] TI, http://www.ti.com.cn/cn/lit/ds/symlink/tms320c6713b.pdf, 2018.

[24] "IEEE standard for synchrophasor measurements for power systems – amendment 1: Modification of selected performance requirements," *IEEE Std C37.118.1a-2014 (Amendment to IEEE Std C37.118.1-2011)*, pp. 1–25, Apr. 2014.

[25] F. Wang, W. Zhao, L. Guo, C. Wang, X. Jiang, and Z. Wang, "Optimal filter design for synchrophasor and frequency measurement," *Proc. CSEE*, vol. 37, no. 22, pp. 6691–6699, Nov. 2017.

[26] M. A. Platas-Garza and J. A. D. L. O. Serna, "Dynamic harmonic analysis through Taylor Fourier transform," *IEEE Trans. Instrum. Meas.*, vol. 60, no. 3, pp. 804–813, Mar. 2011.